Journal of Geomine (2023), 1(2), 81-91
DOI: 10.22077/jgm.2023.6696.1013

Contribution of geostatistical modeling on simulating a geomechanical parameter (case study: GSI in Gol-Gohar open pit iron mine, Kerman, southeastern Iran)

Marzieh Shademan[1], Hadi Farhadian[2]

Recived: 2023 Aug. 16, Revised: 2023 Sep. 02, Online Published: 2023 Sep. 03

ABSTRACT

The successful implementation of the GSI system in numerous global construction projects has proven its capability in giving accurate estimations of the strength of diverse rock formations. The patterned arrangement of GSI values in open-pit mining corresponds to the occurrence of geological rifts. The utilization of geostatistical techniques is effective in comprehending the spread of regionalized factors in each designated research location. Because GSI is a non-additive variable, it may be more beneficial to simulate than estimate it. This is because simulation algorithms can provide results without smoothing. In this work, the theory of regionalized variables was used to analyze and interpret the spatial distribution of GSI values measured at the Gol-Gohar iron mine southeast of Kerman City in Kerman Province, southeastern Iran. Variographic techniques were used to understand and identify the regional behavior and distribution of GSI measurements. Moreover, it is feasible to model the GSI estimations for individual blocks on the pit wall and generate maps to decipher the performance of the localized factors. Such assessments can aid in devising strategies for enhancing the slope stability of pit walls to a maximum extent.

KEYWORDS

Geological Strength Index, Gol-Gohar open pit mines, Non-additive variable, Sequential Gaussian Simulation

I. INTRODUCTION

Considering geologic structures like joints and shear within a moving rock body is crucial when determining the response to external force in combined influence with intact rock blocks. This contrasts to geotechnical investigations which typically use intact rock samples in laboratory testing only. In situ testing is costly and poses issues of reliability, repeatability, and scope. As a result, various systems have been developed to link rock properties with observable rock characteristics, including the Geological Strength Index (GSI) and the widely accepted Hoek-Brown failure criterion for assessing rock properties.

The GSI was introduced by Hoek (1994), Hoek et al. (2000) and Hoek et al. (1992). Hoek et al. (1998) and Marinos and Hoek (2000) expanded the index for weak rock formations in several publications. Following that, Marinos and Hoek (2001) created a chart of geologic strength index particularly suited for uneven rock formations such as flysch, which generally comprise turbulent cycles of robust and weak rocks like sandstone and siltstone, respectively. Marinos et al. (2007) subsequently revised this graph.

The GSI is determined by examining the lithology, surface structure, and condition of rock masses, as well as their discontinuities. This evaluation is done by observing exposed rock in areas such as outcrops, road cuts, tunnels, and drill cores. By assessing the blockiness of the mass and the state of its discontinuities, the index considers the major geologic constraints that define a formation. The GSI is a straightforward tool that can be easily and accurately assessed in the field. As geotechnical engineering continues to develop, experts seek new methods for improving design and addressing uncertainties and variations in soil and rock properties. One approach has been to explore using geostatistics in solving geotechnical engineering problems.

In 1963, French professor Georges Matheron developed a mathematical framework for utilizing geostatistics in determining extractable reserves present in mining resources. Matheron drew inspiration from the pioneering research of South African mining engineer D.G. Krige from the 1950s (Matheron, 1963). Today, it is widely used in the mining and petroleum industries and has been successfully integrated in recent years with remote sensing (Meng et al., 2009; Pardo-Iguzquiza et al., 2011) and geographic information systems (GIS), soil science (Davidović et al., 2010; Emery, 2006; Mendes and Lorandi, 2006; Tavares et al., 2008), rock mechanics (Farhadian, 2021; Farhadian and Nikvar-Hassani, 2020; Marache et al., 2002; Öztürk and Nasuf, 2002; Tavchandjian et al., 1997), and hydrology

[1] Department of Mining and Metallurgical Engineering, Amirkabir University of Technology, Tehran, Iran, [2] Department of Mining Engineering, Faculty of Engineering, University of Birjand, Birjand, Iran
✉ M. Shademan: shademan@aut.ac.ir

(Chowdhury et al., 2010; Dehshibi et al., 2022; Hossain et al., 2007; Jalali et al., 2016).

In spatial studies, geostatistical analysis is a valuable tool for understanding the distribution of regionalized variables. The smoothing effect is an expected outcome of linear kriging methods like ordinary kriging. However, accurately modeling extreme values using linear methods is difficult, especially for the first and last quartiles of a data set. Such variables are considered non-additive and require methods for appreciating and modeling their extreme ranges in geoscience fields. Simulating these variables may prove to be more useful than estimating them. As previously mentioned, GSI is an example of a non-additive variable (Deutsch, 2013; Dunham and Vann, 2007). To account for the inherent bias in estimating a non-additive variable, a simulation algorithm was employed to assess the spatial distribution of GSI in the Gol-Gohar iron mine. This approach is necessary to accurately predict the index for every block of the mine wall and develop a dependable slope stability program.

II. GEOLOGICAL SETTING

The Gol-Gohar iron mine is located southeast of Sanandaj-Sirjan, adjacent to the Zagros zone in Iran. The mining area is 53 km southwest of Sirjan at latitudes 55° 15' to 55° 24' and longitudes 29° 3' to 29° 7'. The structural geological model of the mine was determined by analyzing the tectonic characteristics, remote sensing data of the surrounding region, geological survey data of the mine, and information gathered from the Gol-Gohar mine area.

Various faults can be seen in the studied area, including reverse faults, strike faults, normal faults, and large tensile faults with considerable thickness. The location and prevalence of faults surrounding the No. 1 pit in the Gol-Gohar mine are illustrated in Fig. 1.

The faults are attributed to an underground right-lateral strike fault trending in the NW-SE direction and inclined towards the left. This has caused the formation of a compressed lens shape, whereby the northeast and southwest boundaries are thrust faults dipping towards the northeast and southwest, respectively. A perpendicular structural geological section of the area resembles a flower, shown in Fig. 2.

In bedrock enclosing an ore body, faults often have an east-west trend with a dip of 45 to 80 degrees to the south. These faults almost form a boundary between the ore body and the bedrock. Instability is bound to occur as the faults are angled with the northern benches of the mine and their dip aligns with that of the trenches (Hasanpoor et al., 2010).

III. NON-ADDITIVE VARIABLES

Additivity is the characteristic that enables certain variables to be summed up through a linear average, unlike others that do not possess this property (Dunham and Vann, 2007). To avoid creating bias when calculating an average value for a certain attribute, it is essential to verify its additivity. This applies not only to straightforward arithmetic averages, but also to other linear combinations like weighted averages. Kriging and other widely used spatial estimation techniques rely on weighted averages, assuming that the attribute being estimated is indeed additive.

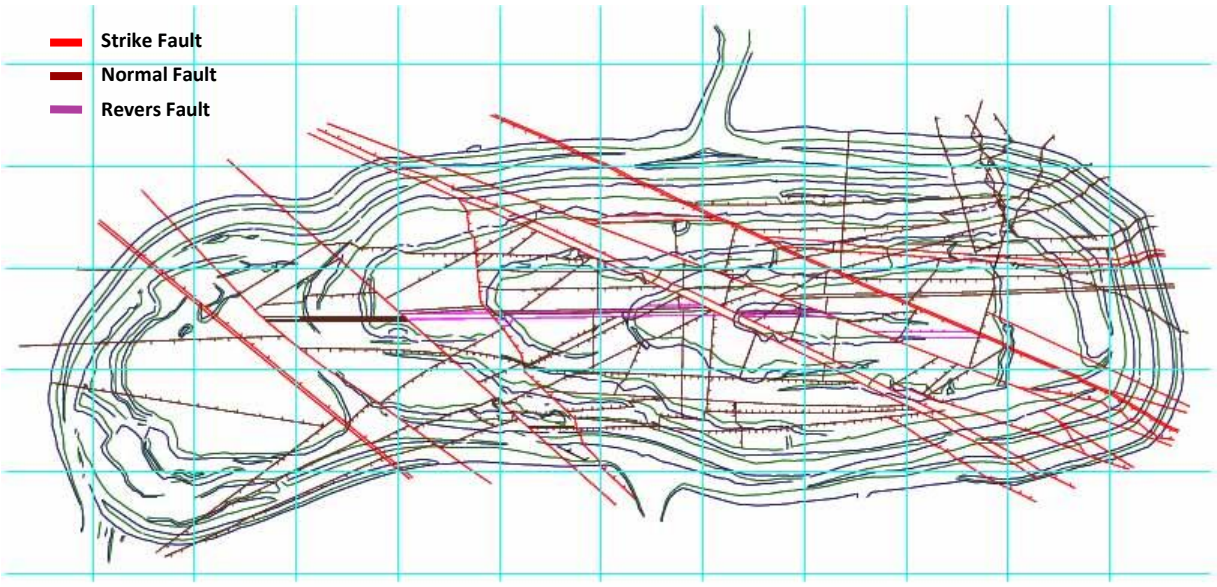

Fig. 1. Faults distribution surrounding pit No.1 of Gol-Gohar iron mine (Hasanpoor et al., (2010).

Fig. 2. Flower faults structure in the southwest wall of the Gol-Gohar mine (Hasanpoor et al., 2010).

Creating of a 3D model to estimate geotechnical attributes like GSI can be compared to creating a grade resource model. However, as opposed to grade variables, the 3D model considers extra non-grade variables linked to each block's actual value. Selecting the appropriate spatial modeling tools is crucial, given that many geomechanical attributes function differently in a spatial context. A well-designed estimation strategy for these new variables is necessary, and in certain cases, simulations can be more useful than estimates that only show local averages. The GSI value's frequency distribution is as important as its absolute value in understanding rock mass properties. GSI is non-additive, and while averaging its values is standard practice, areas with low GSI have a more significant impact on the rock mass's engineering properties. If a spatial modeling approach does not adequately reflect the occurrence of low GSI values, it can lead to making decisions that are not optimal (Deutsch, 2013; Dunham and Vann, 2007).

The linear estimation techniques, such as ordinary kriging, fail to consider the frequency distribution of the output data. While estimating the grade, these approaches smooth out the extreme values, which helps produce unbiased estimates. Nevertheless, relying on these estimates to evaluate engineering design based on smoothed GSI values can be perilous as it might hide the presence of a small zone with low GSI that significantly influences rock performance. Therefore, in such cases, it is advisable to use backward geostatistical tools, particularly geostatistical simulations, to adopt a cautious and impartial approach (Deutsch, 2013; Dunham and Vann, 2007).

Geostatistics is the practical implementation of regionalized variables, where spatial characteristics are treated as random variables. This model views spatial observations as social realizations of a probabilistic function. Although geostatistics is based on a stochastic approach, spatial data is essentially deterministic since it dependents on its location in space. However, the irregularity of its variation necessitates its treatment as random variables. The model is grounded on second-order stationarity, allowing for the spatial modeling of average, variance, and variogram. Nonetheless, Matheron (1971) revealed that second-order stationarity is often too restrictive for many spatial variables, prompting the adoption of the intrinsic hypothesis, which posits stationarity of the average and variance of differences. The theory of regionalized variables is based on the intrinsic hypothesis which assumes quasi-stationarity within a local neighborhood. However, there are situations where the hypothesis does not hold true. In certain regions, the mean values can vary in a predictable or deterministic manner from one part of the region to another. This suggests that there are other factors at play beyond the traditional understanding of regional variability. Further analysis is needed to fully comprehend the complexities of these variable patterns within a region (Chappell et al., 2003). An examination was conducted to assess whether there was a correlation between standard deviation and mean in the area under study. It was determined that there was no noteworthy association between these two variables. To further investigate this, a tool was implemented to look into the spatial regression of the data. Using the parameters of the spatial regression, a simulation algorithm was carried out and analyzed.

IV. METHODOLOGY

The basic geostatistical tool to characterize the spatial variability is the experimental variogram $\gamma(h)$. $\gamma(h)$ is defined as half of the average squared difference for N pairs of measurements of variable z separated by a

distance h (Armstrong, 1998; Cheeney, 1992; Howarth, 1979; Journel and Journel, 1989):

$$\gamma(h) = \frac{1}{2N(h)} \sum_{i=1}^{N(h)} [z(x_i + h) - z(x_i)]^2 \quad (1)$$

Once the experimental variogram has been calculated, it is crucial to select a mathematical model that accurately depicts the spatial variation of the variables. This model must reflects the fluctuations of the variogram concerning the distance h since it will enhance the accuracy and dependability of kriging predictions. Kriging is considered the most efficient and impartial linear estimator for undetermined attributes among the geostatistical methods of interpolation (Cheeney, 1992; Journel and Journel, 1989). By utilizing kriging, one can gain insight into the way natural phenomena behave on a regional level at specific points within a designated study area (Krige, 1962).

If data values are available at specific locations, it is possible to estimate their values at other locations by kriging. The goal of kriging is to predict the average value of the nonadditive variable at the point (x,y,z) summarized as [known as $Z(x_0)$].

The parameter's estimated value at x0 can be determined by using the known values of $Z(x_1). Z(x_2). Z(x_3). \ldots . Z(x_n)$ for the parameter. This is calculated using the formula:

$$Z(x_0) = \sum_{i=1}^{n} w_i Z(x_i) \quad (2)$$

$Z(x_0)$ = the sum of all weights (wi) multiplied by their corresponding Z(xi) values from i = 1 to n. w_i are weights applied to the respective values$Z(x_i)$, such that:

$$\sum_{i=1}^{n} w_i = 1 \quad (3)$$

The weights wi are determined by the Kriging matrix (Cheeney, 1992; Subyani, 1997).

V. Analyzing and Interpreting the Spatial Distribution of GSI Values

In this study, the variable is the GSI obtained from the data measured in geotechnical wells. The location of these boreholes is shown in Fig. 3.

The presented technique aims to demonstrate the regional variation of GSI values. To investigate how the variable of interest is distributed throughout the pit wall, the variogram function is utilized to uncover the regional patterns.

Considering the variogram parameters presented in Table 1, it was found that the GSI data exhibit zonal anisotropy. This anisotropy is seen in the search ellipsoid used for the simulation and is shown in Fig. 4.

The experimental variograms for the GSI data were fitted using spherical models, which are shown in Fig. 5. The optimal threshold and optimal range were selected for each variogram by a cross-validation method.

Regarding the statistical approach to the data set, the range for GSI is wider than that for the interpolated map, and it always makes sense that for the given interpolation algorithm (i.e., kriging) there would be an uninteresting underestimate for high values and an overestimate for low values.

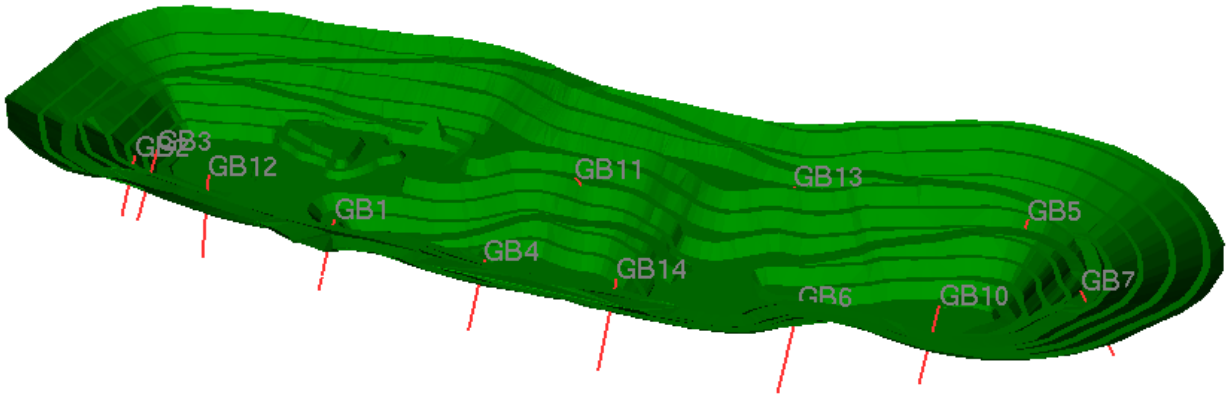

Fig. 3. The location of geotechnical bore holes on the pit wall

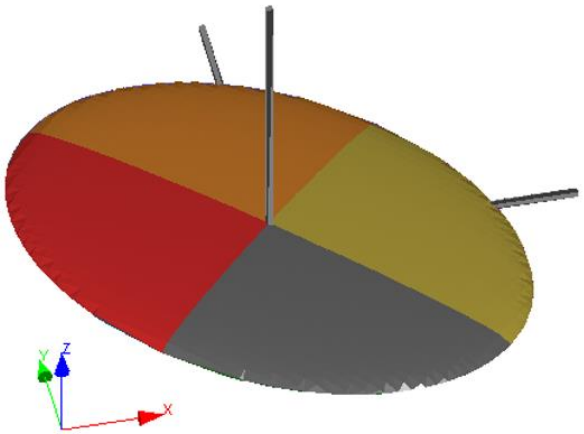

Fig. 4. Search ellipsoid used for simulation of GSI values in the block model

Table 1. The parameters of the variogram functions

Variogram model	Azimuth	Dip	Range(m)	Sill	Nugget
Spherical	-	-	114	80.2	49
Spherical	45	0	374	107.5	20.8
Spherical	135	0	540	118.5	11.9
Spherical	-	90	40	100.8	28.3

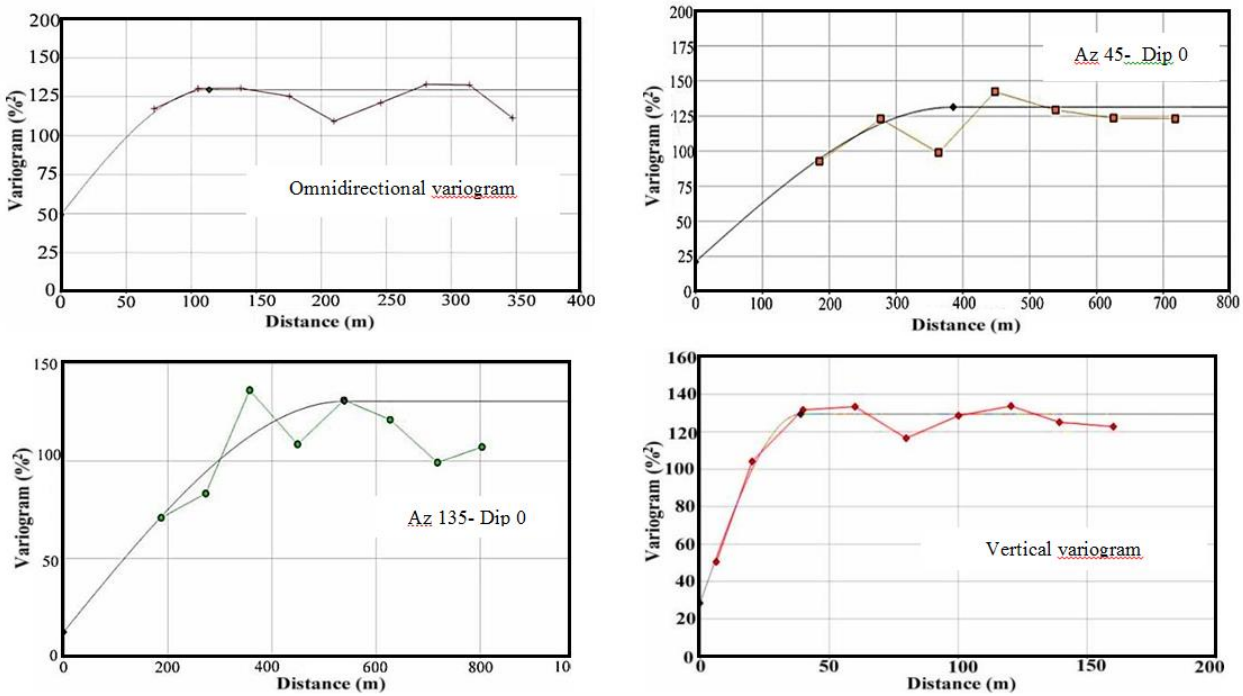

Fig. 5. Spherical model fitted to experimental variograms calculated for GSI values

To simulate or approximate extreme upper and lower values, also known as quartiles, an algorithm must predict these values without a smoothing effect, a negative aspect of some geostatistical methods. Such methods tend to decrease high values and increase low values in order to provide an estimate with the lowest estimation variance. Essentially, inaccurate estimations of secure blocks, which should have high GSI values, as lower than their actual values can result in significant, unnecessary costs to fortify or remove these blocks. Additionally, areas that are anticipated to have low GSI values could be incorrectly assigned higher values, classifying them as moderate or safe instead of as unsafe and critical, thereby exacerbating mining risks.

VI. GEOSTATISTICAL SIMULATION

The utilization of geostatistical simulation tool has progressively become widespread in the numerical representation of natural occurrences that possesses spatial organization. Likewise, the popularity of

simulation tools in geosciences has also surged recently. When dealing with a random variable X, its values are referred to as realizations. Simulating such a variable entail creating random realizations that possess identical mean and variance as the original variable. Alternatively, a random function $Z(x_i)$ comprises numerous RVs for a range of i varying from 1 to n. Subsequently, when considering a random function's realization, it is a compilation of realizations derived from the n RVs components. Therefore, the simulation of a *RF* implies generating a large set of realizations reflecting the characteristic parameters of the considered *RF*. Conditional simulation is the term for the simulation process generating results based on measured values. The use of simulation extends beyond just generating results, it can also be utilized as a spatial interpolator which allows for the calculation of an estimate for an unknown variable at any given point. The estimate calculation involves running the simulation process until the sampled data frequency histogram is replicated, generating a set of realizations for every unsampled point. By averaging these outcomes, an estimate for each point without an actual value can be obtained. Although various methods can simulate one-dimensional RF realizations with a known mean and variance, generalizing these methods to 2 or 3 dimensions poses significant computational difficulties (Barca and Passarella, 2008).

Kriging is a smoothing interpolator that calculates predictions based on weighted moving averages of existing sample data. On the other hand, conditional simulation is not affected by the smoothing effect of kriging. In conditional simulation, the lost variation caused by kriging smoothing is reintroduced through predictions derived from joint realizations of the random variables that are equally likely (Deutsch and Journel, 1992). In other words, the generated figures are not what we anticipated. They are instead chosen randomly from the cumulative distribution function, which takes into consideration the available data and spatial differences predicted by the model (Dungan, 1999).

Simulation enables the creation of numerous scenarios that represent the unpredictability of spatial prediction. These scenarios can serve as a reference to identify possible inaccuracies in estimating the fluctuations of the desired characteristics (Journel, 1996).

Sequential Gaussian simulation (SGS) is likely the most popular technique for carrying out conditional simulation. To avoid biased outcomes, it is essential to ensure that the data being used is distributed normally. Quasi-stationarity properties can be undermined if this criterion is not met. In this kind of simulation, the values generated are dependent on the initial dataset as well as the previously modeled values. The SGS model assumes that all conditional cumulative distribution functions follow a Gaussian distribution (Deutsch and Journel, 1992).

By implementing random numbers, it is possible to vary the sequence in which locations were visited and generate numerous outcomes. This means that when simulated values are added to the existing data set, the potential values available for simulation are partly impacted by previous simulation locations. Hence, the values simulated at a particular location can fluctuate depending on the available data (McKinley et al., 2011).

Generally, when it comes to conditional simulation, it is necessary that the fundamental input parameters, including the spatial model (variograms) and the distribution of sample values (cumulative distribution function, CDF), remain constant across each realization within specific geological interval or facies. However, as each realization begins with a distinct random starting number, it creates a unique "random walk" or path through the 3D or 2D volume. This "random walk" determines the order of cells to be simulated via the simulation algorithm, and it varies between realizations. Consequently, the outcome at unsampled locations differs, producing local alterations in facies distribution and petrophysical properties in interwell space (Torcal et al., 1999). The process of sequential Gaussian simulation is summarized in Fig. 6.

A. Simulation or estimation?

To create accurate simulated data, it is necessary for the values and scattering properties to be replicated (at least up to second order) in the same locations as the real experimental data. However, the goal of conditional simulations differs from estimates. The distinction lies in their respective objectives.

(i) The goal of estimation is to offer an estimator $Z^*(x)$ for every point x that is as accurate as possible to the real, unknown degree $Z_0(x)$. Nevertheless, these estimators may not be able to reflect the spatial fluctuations present in the actual grades $\{Z_0(x)\}$. In the context of kriging, reducing the deviation of the estimation involves smoothing the genuine variances by following the smoothing relationships. Correspondingly, the polygonal influence appraisal method presumes that the grade remains constant across the complete influence polygon of a sample, leading to an inaccurate assessment of the regional variations of the authentic grades. Thus, the estimated deposit $\{Z^*(x)\}$ may provide a prejudiced foundation for investigating the dispersion of real grades.

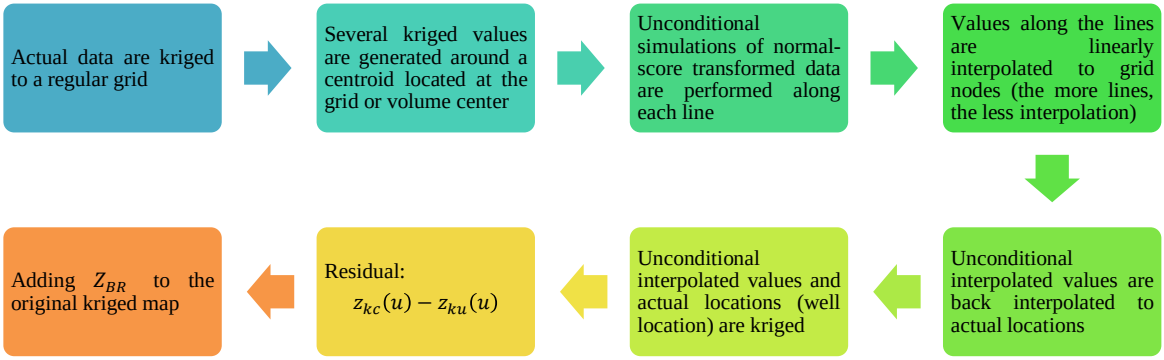

Fig. 6. The process of sequential Gaussian Simulation

(ii) On the other hand, the simulated data ($Z_s(x)$), or better the conditionally simulated data ($Z_{cs}(x)$), have the same first two experimentally determined moments (mean and covariance or variogram, and the histogram) as the real value. On the other hand, the value $Z_s(x)$ or $Z_{cs}(x)$ produced through simulation at each point *x* is not the optimal $Z_0(x)$ estimator. Specifically, the variance of $Z_0(x)$ estimated through conditionally simulated value $Z_{cs}(x)$ is twice the kriging variance. In general, simulating and estimating have opposing objectives (Chiles and Delfiner, 2009).

B. THE PRINCIPLE OF CONDITIONING

Regionalizing a variable $Z_0(x)$ is worth considering, perhaps as the grade at a specific point x. This particular regionalized variable is seen as a manifestation of a stationary RF known as $Z_0(x)$, which has an anticipated mean of m and a centered covariance of $C(h)$ or variogram of $2y(h)$. The goal is to create an RF realization of $Z_{cs}(x)$ that resembles $Z_0(x)$. This means the RF should have the same expected value and second-order moment, $C(h)$ or y(h). Additionally, the RF realization of $Z_{cs}(x)$ should align with the experimental data, which means the simulated and experimental values should match the experimental data points.

$$Z_{cs}(x_0) = Z_0(x), \tag{4}$$

The true value of $Z_0(x)$ and its kriged value $Z_{ok}(x)$,, obtained from the available data $\{Z_0(x)$, where x belongs to I}, should be considered. These two values differ by an unknown error in the form of random functions:

$$Z_0(x) = Z^*_{ok}(x) + [Z_0(x) - Z^*_{ok}(x)] \tag{5}$$

Where, *I* is the range that includes all actual data and is to be kriged or simulated $Z_0(x)$ is the actual value $Z^*_{ok}(x)$ is the estimated value estimated by an ordinary kriging algorithm.

One key feature of kriging is that the difference between the actual value and the predicted value, known as the kriging error $[Z_0(x) - Z^*_{ok}(x)]$, is perpendicular to the predicted values:

$$E\{Z^*_{ok}(x).[Z_0(x) - Z^*_{ok}(x)]\} = 0 \tag{6}$$

Therefore, to obtain the desired conditional simulation, it is sufficient to replace the unknown kriging error in the above formula with an isomorphic and independent kriging error. The conditional simulation that is necessary is subsequently expressed in the following manner:

$$Z^*_{cs}(x) = Z^*_{ok}(x) + [Z_s(x) - Z^*_{sk}(x)] \tag{7}$$

The prerequisites for carrying out a conditional simulation are fulfilled as we possess the subsequent (Chiles and Delfiner, 2009; Deutsch, 2014):

The expected value of $Z_{cs}(x)$ using RF is equal to that of $Z_0(x)$ due to the unbiasedness of the Kriging estimator:

$$E\{Z^*_{ok}(x)\} = E\{Z_0(x)\} \text{ and } E\{Z^*_{sk}(x)\} = E\{Z_s(x)\}$$

which entails

$$E\{Z_{cs}(x)\} = E\{Z_0(x)\} = m \tag{8}$$

This can be explained by the fact that the simulated kriging error and the true error $[Z_0(x) - Z^*_{ok}(x)]$ have an isomorphic relationship with RF $Z_{cs}(x)$. Furthermore, this relationship is not dependent on $Z_{ok}(x)$. It can be observed that the similarity between RF's $Z_{cs}(x)$ and $Z_0(x)$ is only applicable to their increments. This means that while the variograms of these two RFs are the same, their covariance may differ. However, this is not a major issue in geostatistics as the variogram structure function is prioritized over covariance.

The simulated outcome $Z_{cs}(x)$ is linked to the empirical data as the kriging values match the actual values at the data points,

$$Z^*_{ok}(x_0) = Z_0(x_0) \tag{9}$$

Remark 1: The kriging weights for both $Z^*_{ok}(x)$ and $Z^*_{sk}(x)$ are identical because the two random fields, $Z_0(x)$ and $Z_s(x)$, are isomorphic and the kriging setups are identical as well.

Remark 2: The principle of conditioning produces two outcomes for each point x - the kriging $Z^*_{ok}(x)$ and the conditionally simulated $Z^*_{sk}(x)$. As the two kriging errors are independent, the variance of the conditional simulation's estimate of the true value can be expressed as:

$$E\{[Z_0(x) - Z_{sc}(x)]^2\} = E\{[Z_0(x) - Z_{ok}(x)]^2\} + E\{[Z_0(x) - Z_{sk}(x)]^2\} = 2E\{[Z_0(x) - Z_{ok}(x)]^2\} = 2\sigma_k^2 \quad (10)$$

Ultimately, there are five basic steps in the SGS process:

1. Create a random path through the grid nodes.
2. Go to the initial node along the path and utilize Kriging for determining the mean and standard deviation at that node by considering the environmental data, also known as the local conditional probability distribution (lCPD).
3. Choose a value randomly from the lCPD and assign it as the node value.
4. Add the recently generated value to the conditioned data.

According to the given simulation algorithm, several realizations of the GSI dataset were created, and a statistical summary of the simulated GSI is given in Table 2.

The simulated 3D block model of the GSI values with a size of 25×25×10 m is shown in Fig. 7, and the simulated map of the values at the height of 1645 m and the distribution of the errors in the environment can be seen in Fig. 8.

Table 2. Statistical parameters of simulated GSI values and Actual values obtained from drill holes

Field	Parameter	Composites data	Block Model data
GSI%	No of Records	582	35805
	Minimum	0	0
	Maximum	57.5	57.99
	Mean	33.66	33.6
	Skewness	-1.658	-1.688
	Kurtosis	4.225	4.875

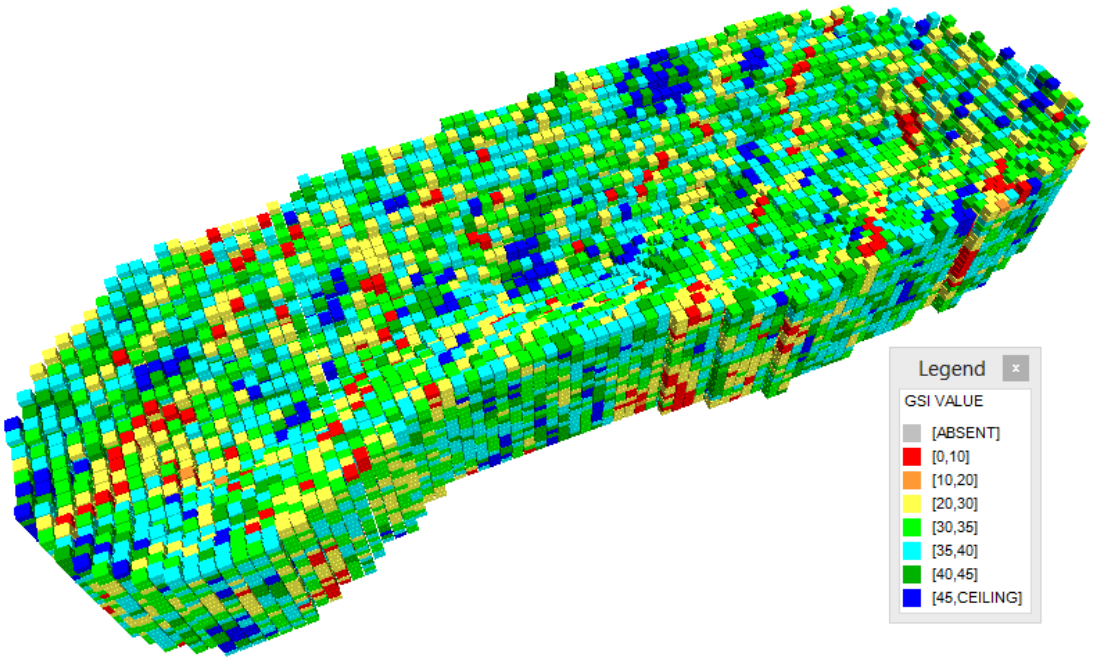

Fig. 7. Block model of simulated GSI values

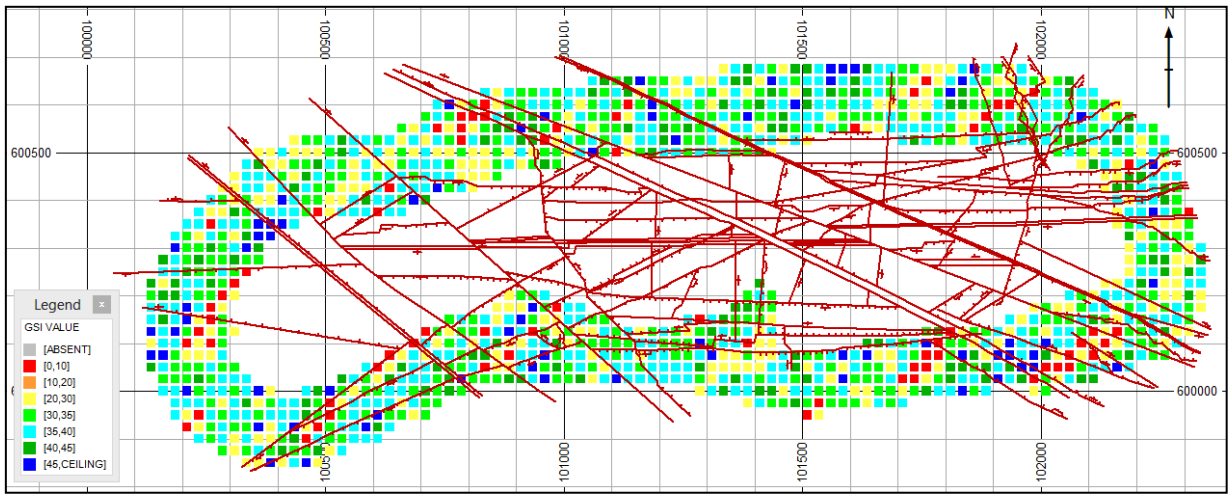

Fig. 8. Simulated map of GSI value at level of 1654m and the distribution of the faults around pit

As can be seen from Figs. 7 and 8, there is a significant relationship between the simulated GSI values and the presence of discontinuities, especially faults in the pit area. To put it differently, the way GSI values are spread out in the Gol-Gohar iron mine No. 1 pit is associated with how discontinuities are spread out. As a result, evaluating the safety factor could be done by considering the covariance between the GSI values and discontinuities in the region. On the other hand, these values could be used to design a maximum slope stability program on pit walls.

C. Validation of Simulated Block Model

Statistical and visual methods are used to validate the simulated block model and are explained below.

D. Visual Validation of Block Model

To visually validate the simulated model, several cross-sections were created. Both the actual values (well data) and the simulated values were plotted to compare the mentioned groups at the common points (Fig. 9 and Fig. 10).

The simulated GSI is compared with the values obtained from boreholes in each vertical section. The results show a satisfactory agreement between the simulated values and the data obtained from the boreholes.

E. Statistical Validation Method

The accuracy of the simulated GSI values was validated by a statistical method. Therefore, a *Q-Q* plot of the simulated and actual values is generated to compare the actual data set with the simulated data set.

A *Q-Q* plot compares the quantiles of a real dataset with those of a simulated dataset. It is a non-parametric method for comparing the distributions of two data samples. The *Q-Q* plot of simulated and actual GSI values demonstrated in Fig. 11 shows proper coincidence between them.

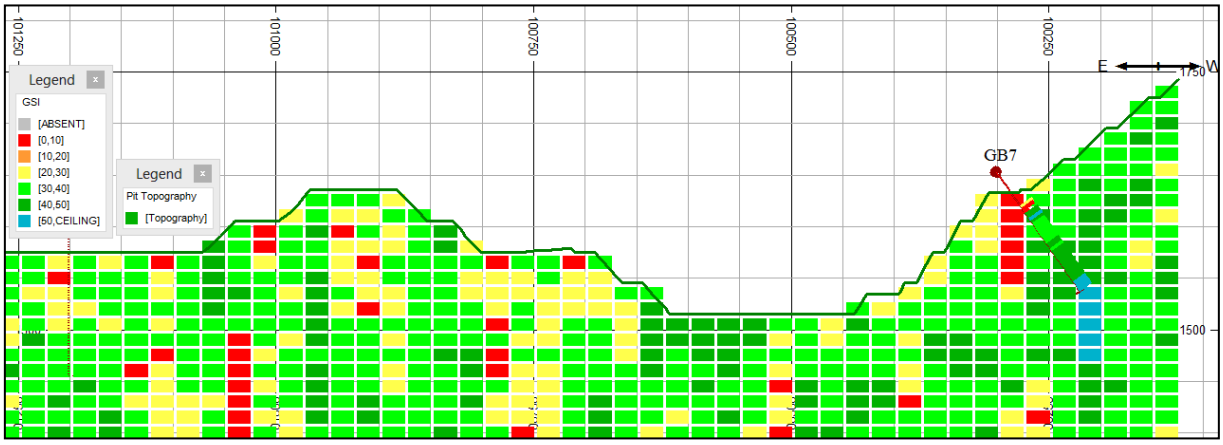

Fig. 9. Visual comparison of simulated and actual values

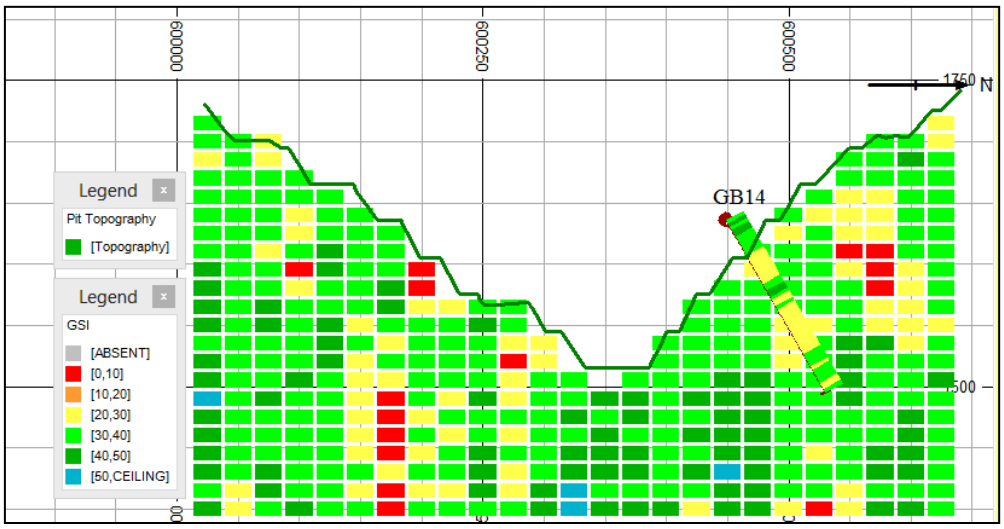

Fig. 10. Visual comparison of simulated and actual values

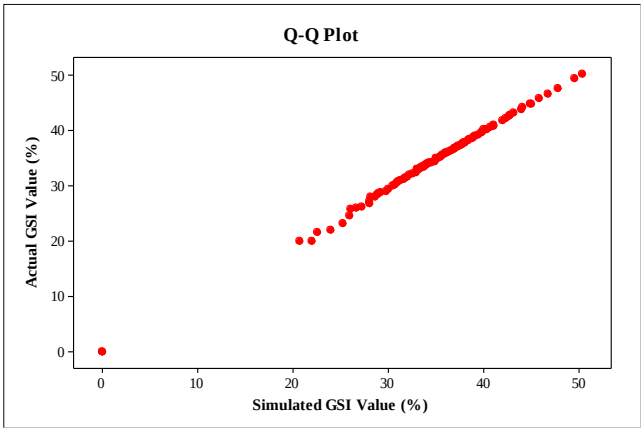

Fig. 11. *Q-Q* plot of simulated and Actual GSI values

VII. CONCLUSION

This research shows that:

1. Geostatistical methods can process uncertainty and modifications in GSI values across different locations in a mine field.

2. To understand the regional behavior of GSI, variogram functions can be determined in the first step of the application. Results from variogram analysis indicate that the spatial structure of GSI has anisotropy in the horizontal surface.

3. To interpret the behavior of the regionalized variable, GSI values can be estimated for each local block on the pit wall and maps can be prepared accordingly.

4. The distribution of GSI values in pit No.1 at the Gol-Gohar iron mine corresponds with the distribution of discontinuities, particularly faults around the pit area.
5. Recognizing and evaluating the spatial relationship of the mentioned index and applying the SGS method of this parameter for all mining walls resulting in a simulated GSI map.

REFERENCE

Armstrong M. (1998). Basic linear geostatistics. Springer Science & Business Media.

Barca E, Passarella G. (2008). Spatial evaluation of the risk of groundwater quality degradation. A comparison between disjunctive kriging and geostatistical simulation. Environ Monit Assess. 137, 261–73.

Chappell A, Heritage GL, Fuller IC, Large ARG, Milan DJ. (2003). Geostatistical analysis of ground-survey elevation data to elucidate spatial and temporal river channel change. Earth Surf Process Landforms J Br Geomorphol Res Gr. 28, 349–70.

Cheeney, R.F., E.H., Isaaks, Srivastava R.M. (1990). An Introduction to Applied Geostatistics. xix+ 561 pp. New York, Oxford: Oxford University Press. Price£ 19.50 (paperback). ISBN 0 19 505013 4. Geol Mag. 129, 125–6.

Chiles, J.P., Delfiner, P. (2012). Geostatistics: modeling spatial uncertainty (Vol. 713). John Wiley & Sons.

Chowdhury, M., Alouani, A., Hossain, F. (2010). Comparison of ordinary kriging and artificial neural network for spatial mapping of arsenic contamination of groundwater. Stoch Environ Res Risk Assess. 24, 1–7.

Davidović, N., Prolović, V., Stojić, D. (2010). Modeling of soil parameters spatial uncertainty by geostatistics. Facta Univ Archit Civ Eng. 8, 111–8.

Dehshibi, R., Karami, S., Maleki, Z., Farhadian, H. (2022). A comparative study on evaluation of steady-state groundwater quality in Sirjan's Golgohar mineral zone. Arab J Geosci. 15, 1–20.

Deutsch, C.V. (2013). Geostatistical modelling of geometallurgical variables—Problems and solutions. Proc. Int. Geometallurgy Conf. Brisbane, Aust., 30.

Deutsch, C.V., Journel, A.G. (1992). Geostatistical software library and user's guide. Oxford Univ Press. 8,0-1.

Deutsch, J.L. (2015). Experimental variogram tolerance parameters. Geostatistics Lessons, http://www. geostatisticslessons. com/lessons/variogramparameters.

Dungan, J.L. (1999). Conditional simulation: An alternative to estimation for achieving mapping objectives. In Spatial statistics for remote sensing (pp. 135-152). Dordrecht: Springer Netherlands.

Dunham, S., Vann, J. (2007, June). Geometallurgy, geostatistics and project value—does your block model tell you what you need to know. In Proceedings of the Project Evaluation Conference, Melbourne, Australia (pp. 19-20).

Emery, X. (2006). Ordinary multigaussian kriging for mapping conditional probabilities of soil properties. Geoderma, 132(1-2), 75-88.

Farhadian, H. (2021). A new empirical chart for rockburst analysis

in tunnelling: Tunnel rockburst classification (TRC). International Journal of Mining Science and Technology, 31(4), 603-610.

Farhadian, H., Nikvar-Hassani, A. (2020). Development of a new empirical method for Tunnel Squeezing Classification (TSC). Quarterly Journal of Engineering Geology and Hydrogeology, 53(4), 655-660.

Hasanpoor, J., Tarigh Azali, S., Sadeghi, S.H. (2010). Report of Structural geology and geological study of pit No. 1 of Gol-e-Gohar mine. GoleGohar Iron Ore Co, 2.

Hoek E. Strength of rock and rock masse, 1994.

Hoek, E., Kaiser, P.K., Bawden, W.F. (2000). Support of underground excavations in hard rock. CRC Press.

Hoek, E., Marinos, P., Benissi, M. (1998). Applicability of the Geological Strength Index (GSI) classification for very weak and sheared rock masses. The case of the Athens Schist Formation. Bull Eng Geol Environ, 57, 151–60.

Hoek, E., Wood, D., Shah, S. (1992). A modified Hoek–Brown failure criterion for jointed rock masses. Rock Charact. ISRM Symp. Eurock'92, Chester, UK, 14–17 Sept. 1992, Thomas Telford Publishing, p. 209–14.

Hossain, F., Hill, J., Bagtzoglou, A.C. (2007). Geostatistically based management of arsenic contaminated ground water in shallow wells of Bangladesh. Water Resour Manag, 21, 1245–61.

Howarth, R.J. (1979). Journel and (Ch. J.) Huijbregts. Mining Geostatistics. London & New York (Academic Press), 1978. x+ 600 pp., 267 figs. Price£ 32· 00. Mineralogical Magazine, 43(328), 563-564.

Jalali, M., Karami, S., Marj, A.F. (2016). Geostatistical evaluation of spatial variation related to groundwater quality database: case study for Arak plain aquifer, Iran. Environ Model Assess, 21, 707–19.

Journel, A.G. (1996). Modelling uncertainty and spatial dependence: stochastic imaging. Int J Geogr Inf Syst, 10, 517–22.

Journel, A.G., Journel, A.G. (1989). Fundamentals of geostatistics in five lessons (Vol. 8). Washington, DC: American Geophysical Union.

Krige, D.G. (1962). Statistical applications in mine valuation.

Marache, A., Riss, J., Gentier, S., Chilès, J. (2002). Characterization and reconstruction of a rock fracture surface by geostatistics. Int J Numer Anal Methods Geomech, 26, 873–96.

Marinos, P., Hoek, E. (2001). Estimating the geotechnical properties of heterogeneous rock masses such as flysch. Bull Eng Geol Environ, 60, 85–92.

Marinos, P., Hoek, E. (2000, November). GSI: a geologically friendly tool for rock mass strength estimation. In ISRM international symposium (pp. ISRM-IS). ISRM.

Marinos, P.G., Marinos, V., Hoek, E. (2007). The geological strength index (GSI): A characterization tool. In Proceedings of the international workshop on rock mass classification in underground mining (No. 9498, p. 87). Deptartment of Health and Human Services, Centers for Disease Control and Prevention, National Institute for Occupational Safety and Health, Pittsburgh Research Laboratory.

Matheron, G. (1971). The theory of regionalised variables and its applications. Les Cah Du Cent Morphol Mathématique, 5, 212.

Matheron, G. (1963). Principles of geostatistics. Econ Geol, 58, 1246–66.

McKinley, J.M., Atkinson, P.M., Lloyd, C.D., Ruffell, A.H., Worden, R.H. (2011). How porosity and permeability vary spatially with grain size, sorting, cement volume, and mineral dissolution in fluvial Triassic sandstones: the value of geostatistics and local regression. J Sediment Res, 81, 844–58.

Mendes, R.M., Lorandi, R. (2006). Indicator kriging geostatistical methodology applied to geotechnics project planning. IAEG2006 Pap, 527, 1–12.

Meng, Q., Cieszewski, C., Madden, M. (2009). Large area forest inventory using Landsat ETM+: a geostatistical approach. ISPRS J Photogramm Remote Sen, 64, 27–36.

Öztürk, C.A., Nasuf, E. (2002). Geostatistical assessment of rock zones for tunneling. Tunn Undergr Sp Technol, 17, 275–85.

Pardo-Iguzquiza, E., Rodríguez-Galiano, V.F., Chica-Olmo, M., Atkinson, P.M. (2011). Image fusion by spatially adaptive filtering using downscaling cokriging. ISPRS J Photogramm Remote Sens, 66, 337–46.

Subyani, A.M. (1997). Geostatistical analysis of precipitation in southwest Saudi Arabia. Colorado State University.

Tavares, M.T., Sousa, A.J., Abreu, M.M. (2008). Ordinary kriging and indicator kriging in the cartography of trace elements contamination in São Domingos mining site (Alentejo, Portugal). J Geochemical Explor, 98, 43–56.

Tavchandjian, O., Rouleau, A., Archambault, G., Daigneault, R., Marcotte, D. (1997). Geostatistical analysis of fractures in shear zones in the Chibougamau area: applications to structural geology. Tectonophysics, 269(1-2), 51-63.

Torcal, F., Posadas, A. M., Chica, M., Serrano, I. (1999). Application of conditional geostatistical simulation to calculate the probability of occurrence of earthquakes belonging to a seismic series. Geophysical Journal International, 139(3), 703-725.